Front. Mech. Eng. 2022, 17(2): 16
https://doi.org/10.1007/s11465-022-0672-8

RESEARCH ARTICLE

Thermal analysis of lubricated three-dimensional contact bodies considering interface roughness

Jiqiang WU[a], Liqin WANG (✉)[a,b], Zhen LI[a], Peng LIU[a], Chuanwei ZHANG[a]

[a] *MIIT Key Laboratory of Aerospace Bearing Technology and Equipment, Harbin Institute of Technology, Harbin 150001, China*
[b] *State Key Laboratory of Robotics and System, Harbin Institute of Technology, Harbin 150080, China*
✉ *Corresponding author. E-mail: lqwanghit@163.com (Liqin WANG)*

ABSTRACT Surface roughness and thermal action are of remarkable importance in the lubrication performance of mechanical components, especially in extreme conditions. However, available studies mainly focus on the full-film lubrication conditions without considering temperature rise and real 3D surface roughness due to the complexity of surface topography and temperature characteristics. Moreover, studies on the interfacial thermal behaviors of 3D rough surface lubricated contact in an extended range of working conditions remain limited. In this paper, a deterministic mixed thermal elastohydrodynamic lubrication model considering real 3D surface roughness and thermal effects is proposed. In this model, pressure and temperature are coupled with each other, the computation of elastic deformation is accelerated through the discrete convolution and fast Fourier transform method, the temperature field is calculated with the column sweeping technique, and the semi-system method is introduced to improve convergence and numerical stability under severe conditions. The model is validated by comparing its results with available published numerical and experimental results. The thermal behaviors of the contact interface are studied in a wide range of working conditions. The influences of surface roughness and thermal effect on lubrication performance are revealed. The results show that the proposed model can be used as a powerful analysis tool for lubrication performance and temperature prediction in various heavy-load, high-speed lubricated components over a wide range of lubrication conditions.

KEYWORDS thermal elastohydrodynamic lubrication, surface roughness effect, thermal effect, temperature characteristics, severe conditions

1 Introduction

Thermal effects have an important influence on the performance of heavy-load, high-speed lubricated components such as aero-engine main shaft bearings and aircraft gears. For these extreme running conditions, temperature is substantially increased, and this may lead to thin lubricant film and even mixed and boundary lubrication in roughness surface contacts. The poor lubrication status may cause large friction, massive wear, and local high temperature, resulting in surface failure and life reduction. Therefore, a good understanding of temperature characteristics is crucial for the reduction of lubrication failure, improvement of reliability, and optimization design of components.

Considerable progress has been made in the theoretical analysis of thermal elastohydrodynamic lubrication (TEHL) over the past decades after the study on the TEHL in line contacts by Cheng and Sternlicht [1]. Zhu and Wen [2] presented the first full numerical solution for TEHL elliptical contacts at relatively low loads. Kim and Sadeghi [3] provided a solution for the point-contact TEHL problem under higher load conditions using multigrid technology. Yang et al. [4–6] improved the multigrid method and used the Newtonian flow model to analyze thermal actions on film thickness. Kim et al. [7], Liu et al. [8], Cui et al. [9], and others then studied coupled non-Newtonian behaviors and thermal effects on lubrication characteristics. Liu et al. [10] established a model for the TEHL of layered materials under line contact cases and studied the thermal behaviors of oil film and coating bodies. Habchi [11] proposed a finite element model for the TEHL of finite length contacts and discussed the influences of roller profiles on lubrication performance. He et al. [12] developed a thermal–visco–

Received July 25, 2021; accepted January 10, 2022

elastohydrodynamic lubrication model and numerically studied the effects of temperature rise on lubrication behaviors under different conditions. However, most of the said TEHL studies are limited to the calculations of lubricant full film condition with smooth surfaces. The contacting surfaces are rough and usually operate in the mixed lubrication state owing to direct asperity contacts. Hence, the roughness effect is important and must be considered during the analysis of TEHL performance. Other than the research work above, numerical studies have also been conducted on the problems of surface contact thermal analysis with start-up process [13], multilayered material [14], inhomogeneous material [15], and interfacial slip [16].

Owing to the limited computer technologies in early years, the studies of mixed lubrication mainly focused on stochastic models [17–19]. Limited stochastic parameters were used to describe the rough surface and lubrication performance, but the detailed local film thickness fluctuations and pressure peaks at the contact interface cannot be obtained, which limits the further understanding of lubrication failure mechanisms. Then, increased attention was turned to the deterministic mixed elastohydrodynamic lubrication (EHL) model. A converged, accurate deterministic solution for rough surface mixed lubrication has always constituted a challenge for lubrication studies due to the complexity of surface roughness. Previous deterministic rough surface lubrication analyses were mainly conducted with simple artificial roughness or 2D machined rough surfaces [20–22]. When realistic 3D rough surface was considered in lubrication studies, the lubrication systematic equations showed a strong nonlinear behavior and the constructed coefficient matrix was often singular, especially in harsh lubrication situations with ultrathin films or existing asperity contacts. With the available semi-system numerical method presented by Ai [23], Hu and Zhu [24] first published a united mixed EHL model to characterize the 3D real machined roughness point contact problems, which can simulate all the lubrication regions including boundary and mixed lubrication as well as full film EHL. Since then, He et al. [25–28] improved this model to consider the effects of plastic deformation and surface coating. Pu et al. [29,30] developed a mixed EHL model of elliptical contacts considering an arbitrary entrainment angle. Gan et al. [31] coupled the finite element method with a mixed EHL model to investigate the temperature behavior of spiral bevel gears under mixed lubrication conditions. Chen et al. [32] investigated the mixed lubrication computation problem by using a new iterative method based on Crank–Nicolson integration. However, these mixed lubrication studies were based on isothermal conditions. For mixed TEHL studies with rough surfaces, Wang et al. [33,34] investigated the thermal effects on pressure distributions through a transient mixed TEHL model. Yan et al. [35] studied the influences of surface roughness and spinning on lubrication characteristics and fatigue life under mixed TEHL conditions. In their models, the calculation of the temperature field is solved by the simplified 2D oil film energy equation with surface temperature equations. This approach may not provide accurate predictions of temperature distributions, especially for extreme conditions. Wang et al. [36] used a 3D energy equation of oil film and surface temperature equations to present a point contact mixed TEHL model and analyzed the rough surface lubrication performance under different lubrication conditions. However, the influences of working conditions on the detailed temperature behaviors of the contact interface (such as the temperature in the inlet, contact zone, and outlet) are not studied. The change in temperature characteristics at different working conditions remains not well understood.

Thus, this work aims to develop a more realistic deterministic mixed TEHL model for 3D thermal elastohydrodynamically lubricated contacts by considering thermal effects and real 3D surface roughness, and presents a detailed investigation on the film thickness, pressure, and oil film and solid temperature behaviors in a wide range of working conditions. The present numerical model is an extension of the mixed deterministic mixed EHL model [24,37] by combining the unified equations for mixed EHL model and energy equations for oil film and solids, which can simulate the entire transition of interfacial status with real 3D roughness involved. It can be employed to provide technical support for predicting the lubrication performance and temperature of various heavy-load, high-speed lubricated components in aerospace applications. The model is validated with available published data. The thermal behaviors of the 3D rough surface lubricated contact interface are then carried out over a wide range of working conditions, and the surface roughness and thermal effects on the lubrication characteristics are investigated. The obtained mixed TEHL performance covers all lubrication statuses. This work can provide a theoretical basis for the judgment of lubrication state and failure analysis in extreme conditions.

2 Theoretical method

2.1 Description of mixed TEHL model

A deterministic mixed isothermal EHL model with a unified equation system and numerical approach that can simulate the entire lubrication status [24,37] is extended for analyzing the mixed TEHL characteristics in elliptical contacts. Such typical contacts can be found in various ball bearings. The geometry and computational domain for an elliptical contact problem are given in Fig. 1. x, y, z, z_1, and z_2 represent the corresponding coordinates. d

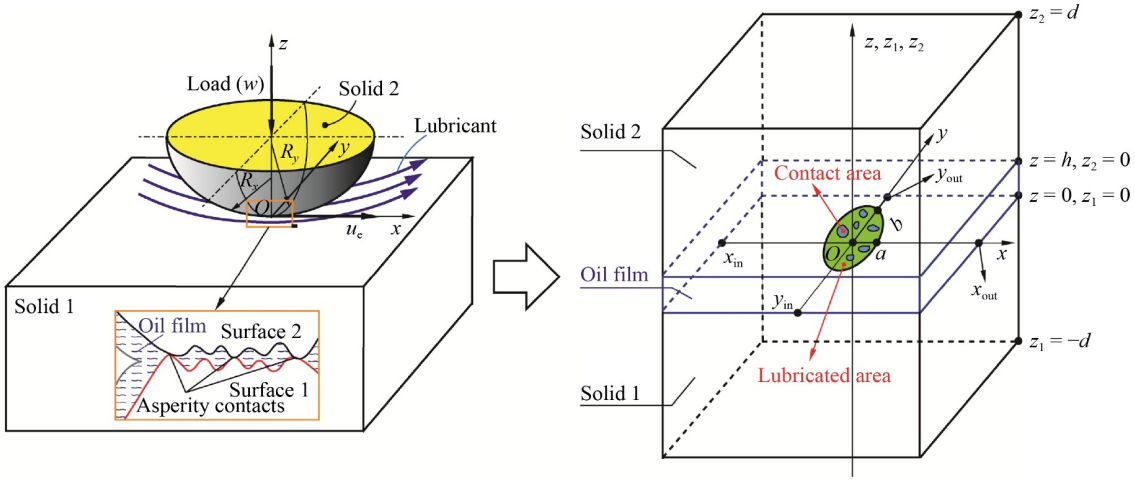

Fig. 1 Geometry and computational domain of mixed TEHL in an elliptical contact.

indicates the thickness of the temperature calculation domain in each solid. w is the applied load. $u_e = (u_1+u_2)/2$ is the entrainment velocity, where u_1 and u_2 indicate the velocities of surfaces 1 and 2, respectively. Both rough surfaces run in the x direction. R_x and R_y denote the equivalent radii of the two surfaces in the x and y directions, respectively. a and b represent the semi axis Hertzian contact ellipse in the x and y directions, respectively.

To simplify the solution and reduce the computing time in the calculation of pressure under thermal conditions, the changes of viscosity and density across the lubricant film are neglected and computed based on the mean temperature of the oil film [38]. Moreover, the contact becomes a transient problem because the moving rough surfaces cause the change of microgeometry. Hence, the transient squeezing effect is considered in the Reynolds equation. The transient Reynolds equation for thermal analyses is given by the following:

$$\frac{\partial}{\partial x}\left(\frac{\rho h^3}{12\eta^*}\frac{\partial p}{\partial x}\right)+\frac{\partial}{\partial y}\left(\frac{\rho h^3}{12\eta^*}\frac{\partial p}{\partial y}\right)=u_e\frac{\partial(\rho h)}{\partial x}+\frac{\partial(\rho h)}{\partial t}, \quad (1)$$

where p and h correspond to the pressure and film thickness, respectively, and ρ denotes the lubricant density. Furthermore, the lubricant non-Newtonian behavior is considered by introducing an effective viscosity η^*, which is computed as follows [9]:

$$\frac{1}{\eta^*}=\frac{1}{\eta}\frac{\tau_0}{\tau}\sinh\frac{\tau}{\tau_0}, \quad (2)$$

where η denotes the lubricant viscosity, and τ and τ_0 represent the shear stress and characteristic shear stress, respectively.

The boundary and cavitation conditions for solving the Eq. (1) can be written as follows:

$$\begin{cases} p(x_{in},y,t)=p(x_{out},y,t)=p(x,y_{in},t)=p(x,y_{out},t)=0, \\ p(x,y,t)\geqslant 0 \quad (x_{in}<x<x_{out},\ y_{in}<y<y_{out}), \end{cases} \quad (3)$$

where x_{in} and x_{out} represent the inlet and outlet edges in the x direction, respectively, and y_{in} and y_{out} represent the inlet and outlet edges in the y direction, respectively.

The viscosity–pressure–temperature relationship of the lubricant can be described by Roelands equation [39]:

$$\begin{cases} \eta=\eta_0\exp\left\{(\ln\eta_0+9.67)\right. \\ \qquad \left.\cdot\left[-1+(1+5.1\times10^{-9}p)^{z_0}\left(\dfrac{T-138}{T_0-138}\right)^{-s_0}\right]\right\}, \\ z_0=\dfrac{\alpha}{5.1\times10^{-9}(\ln\eta_0+9.67)}, \\ s_0=\dfrac{\gamma(T_0-138)}{\ln\eta_0+9.67}, \end{cases} \quad (4)$$

where η_0 denotes the ambient viscosity of lubricant, T and T_0 represent the temperature and ambient temperature, respectively, z_0 and s_0 are the coefficients for Roelands equation, α denotes the viscosity–pressure coefficient, and γ represents the viscosity–temperature coefficient.

The density–pressure–temperature relationship of the lubricant can be described by Dowson and Higginson equation [40]:

$$\rho=\rho_0\left[1+\frac{0.6\times10^{-9}p}{1+1.7\times10^{-9}p}-\beta(T-T_0)\right], \quad (5)$$

where ρ_0 is the ambient density of lubricant, and β is the thermal expansion coefficient of lubricant.

Lubricant film thickness is computed by

$$h(x,y,t)=h_0(t)+\frac{x^2}{2R_x}+\frac{y^2}{2R_y}+\delta_1(x,y,t)+\delta_2(x,y,t)+V_e(x,y,t), \quad (6)$$

where $h_0(t)$ denotes the rigid body central distance, and $\delta_1(x, y, t)$ and $\delta_2(x, y, t)$ represent the roughness heights of the two surfaces, which change with time and can be expressed as follows:

$$\begin{cases}\delta_1(x,y,t)=s_1(x-u_1t,y),\\ \delta_2(x,y,t)=s_2(x-u_2t,y),\end{cases} \tag{7}$$

where $s_1(x, y)$ and $s_2(x, y)$ denote the discretized roughness height data matrix of surfaces 1 and 2, respectively.

$V_e(x, y, t)$ indicates the elastic deformation that can be calculated through the Boussinesq integration:

$$V_e(x,y,t)=\frac{2}{\pi E'}\iint_{\Omega}\frac{p(\xi,\varsigma,t)}{\sqrt{(x-\xi)^2+(y-\varsigma)^2}}\mathrm{d}\xi\mathrm{d}\varsigma, \tag{8}$$

where E' indicates the effectively elastic modulus, ξ and ς indicate the x and y coordinates of pressure when calculating deformation, respectively.

The load balance equation is expressed as follows:

$$w=\iint_{\Omega}p(x,y,t)\,\mathrm{d}x\mathrm{d}y. \tag{9}$$

In the mixed TEHL model, the calculation of temperature for the oil film is divided by the lubricated regions and asperity contact regions. The oil film energy equation in the lubricated regions can be formulated as follows [41]:

$$\begin{aligned}&c_f\rho\left[\frac{\partial T}{\partial t}+u\frac{\partial T}{\partial x}+v\frac{\partial T}{\partial y}+q\frac{\partial T}{\partial z}\right]-k_f\frac{\partial^2T}{\partial z^2}\\&=-\frac{T}{\rho}\frac{\partial\rho}{\partial T}\left(\frac{\partial p}{\partial t}+u\frac{\partial p}{\partial x}+v\frac{\partial p}{\partial y}\right)+\eta^*\left[\left(\frac{\partial u}{\partial z}\right)^2+\left(\frac{\partial v}{\partial z}\right)^2\right],\end{aligned} \tag{10}$$

where c_f denotes the specific heat of lubricant, k_f represents the thermal conductivity of lubricant, and u, v, and q denote the components of lubricant velocity in the x, y, and z directions, respectively.

When the film thickness approaches zero, the asperity contacts take place and the terms of heat convection and compressive heat can be neglected due to the disappearance of lubricant flow. Thus, the oil film energy equation is reduced to the following [42]:

$$k_f\frac{\partial^2T}{\partial z^2}=f_b\frac{u_2-u_1}{h_b}p, \tag{11}$$

where f_b is the boundary lubrication friction coefficient, and h_b is the boundary film thickness.

The energy equations for the two solids are expressed as follows:

$$\begin{cases}c_1\rho_1\left(\dfrac{\partial T}{\partial t}+u_1\dfrac{\partial T}{\partial x}\right)=k_1\dfrac{\partial^2T}{\partial z_1^2},\\ c_2\rho_2\left(\dfrac{\partial T}{\partial t}+u_2\dfrac{\partial T}{\partial x}\right)=k_2\dfrac{\partial^2T}{\partial z_2^2},\end{cases} \tag{12}$$

where c_1 and c_2 indicate the specific heats of bodies 1 and 2, respectively, ρ_1 and ρ_2 represent the densities of bodies 1 and 2, respectively, and k_1 and k_2 denote the thermal conductivities of bodies 1 and 2, respectively.

The boundary conditions of energy equations are as follows:

$$\begin{cases}T(x_{in},y,z,t)=T_0, \quad u(x_{in},y,z,t)\geqslant 0,\ z\in[0,h],\\ T(x_{in},y,z_1,t)=T_0, \quad z_1\in[-d,\ 0],\\ T(x_{in},y,z_2,t)=T_0, \quad z_2\in[0,\ d],\\ T(x,y,-d,t)=T(x,y,d,t)=T_0, \quad x\in[x_{in},\ x_{out}].\end{cases} \tag{13}$$

On the two solid–liquid interfaces, heat flux continuity conditions must be satisfied:

$$\begin{cases}k_f\left.\dfrac{\partial T}{\partial z}\right|_{z=0}=k_1\left.\dfrac{\partial T}{\partial z_1}\right|_{z_1=0},\\ k_f\left.\dfrac{\partial T}{\partial z}\right|_{z=h}=k_2\left.\dfrac{\partial T}{\partial z_2}\right|_{z_2=0}.\end{cases} \tag{14}$$

2.2 Numerical procedure

The solution for the mixed TEHL model mainly consists of two parts: the pressure iteration of the Reynolds equation and the temperature iteration of the oil thickness and solid energy equations with their boundary conditions. Figure 2 shows the numerical calculation flowchart for mixed TEHL analysis. At the beginning of the analysis, the input parameters include the working conditions, solid materials and lubricant properties, and geometry parameters as well as initial pressure, film thickness, and temperature distributions. In the pressure iteration loop, the semi-system approach is employed to solve the Reynolds equation. With this method, the h in the entrainment flow term of Reynolds equation $(\partial(\rho h)/\partial x)$ is also considered a function of unknown nodal pressure. Thus, the coefficient matrix is constructed with the pressure flow terms and additional entrainment flow term, and the diagonal dominance of the equation can be ensured even when the pressure flows become very weak. This method has shown good convergence and stability for ultra-thin film and mixed lubrication cases with rough surfaces involved, even under extreme operating conditions [23,24,37]. The lubricant viscosity and density in the pressure equation are evaluated based on the updated pressure and the mean temperature of oil film $\left(T_m=\frac{1}{h}\int_0^h T\mathrm{d}z\right)$ [38]. Furthermore, the discrete convolution and fast Fourier transform technique [43,44] is introduced to accelerate the elastic deformation computation. Next, the oil film and solid energy equations are solved through the column sweeping approach [5,45] to obtain the temperature field. This approach has been proven to improve the convergence solution for temperature with the severe reverse flow of the oil film. Pressure and temperature are solved by turns until the pressure, load balance, and temperature converge to certain precision simultaneously: $\varepsilon_p=\sum\sum\left|p_{ij}^{new}-p_{ij}^{old}\right|/\sum\sum p_{ij}^{new}\leqslant 1\times10^{-4}$, $\varepsilon_w=\left|\sum\sum p_{ij}^{new}-w\right|/w\leqslant 1\times10^{-3}$, and $\varepsilon_T=\sum\sum\sum\left|T_{ijk}^{new}-T_{ijk}^{old}\right|/\sum\sum\sum T_{ijk}^{new}\leqslant 1\times10^{-4}$, where ε_p, ε_w, and ε_T are the convergence factors of pressure, load, and temperature, respectively. Then, the computation is

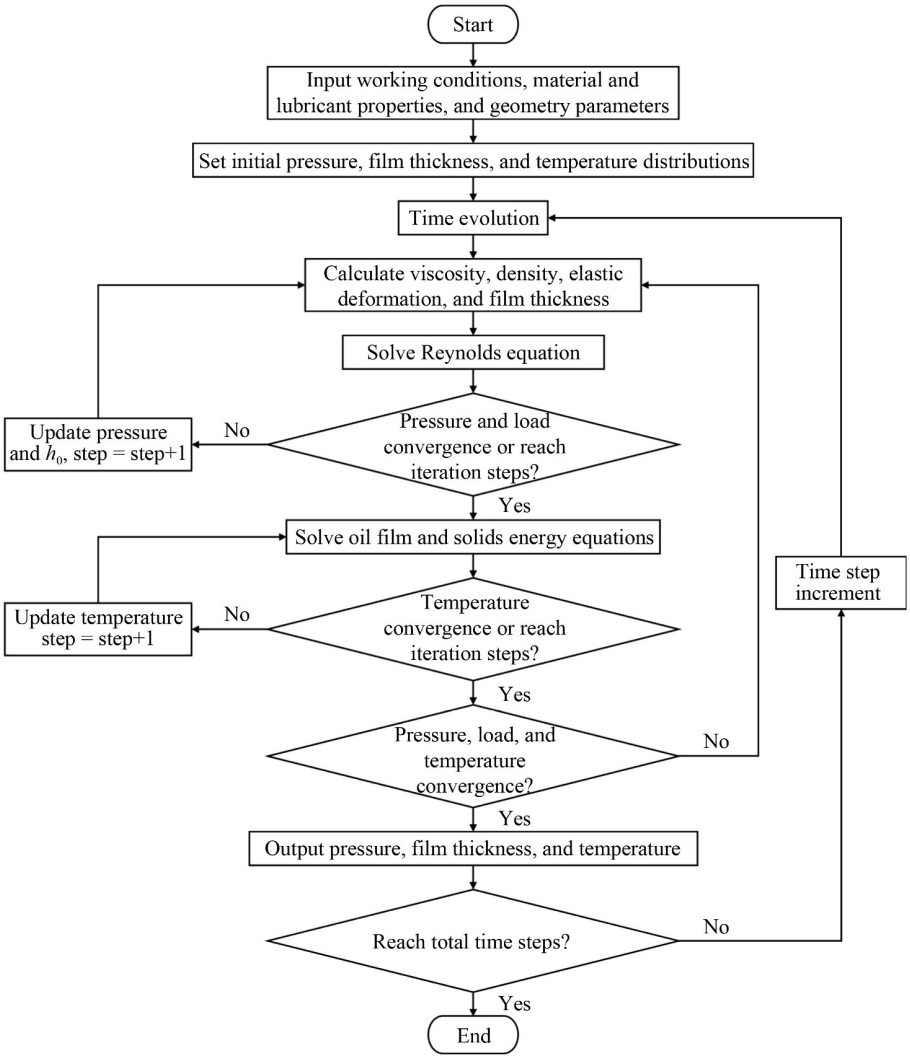

Fig. 2 Numerical calculation flowchart for solving the mixed TEHL problem.

carried out in the next time step. After running in a sufficient number of time steps, a globally stabilized solution can be obtained.

3 Model validation

To validate the current model, its smooth solutions are compared with the numerical and experimental results from the literature. The first comparison is made between the numerical results obtained from the current model and those published in Ref. [46]. For this validation case, a steel ball of 12.7 mm in radius is loaded at 39.2 N against a glass disc. The entrainment velocity is 0.36 m/s with the slide–roll ratio (*SRR*) of −1.0. The contacting bodies and lubricant properties corresponding to Ref. [46] are given in Table 1. The obtained pressure, film thickness, and temperature distributions plotted in Fig. 3 agree with the previous results of Kaneta et al. [46]. In Fig. 3, T_{mid}, T_g, and T_s indicate the temperature distributions in the central film and on the surfaces of the glass disc and the steel ball, respectively. The pressure and film thickness profiles have the typical characteristics of EHL, the pressure peak and minimum film thickness at the outlet area can be clearly observed. As for the temperature distributions, the temperature on the glass surface is much higher than that on the steel surface because of the lower thermal conductivity of glass compared with steel.

The second comparison is made with the corresponding experiment results in Ref. [47]. The analyzed parameters are kept the same with the experiment in Ref. [47] are: w = 20 N, E' = 117 GPa, p_h = 0.526 GPa, R_x = 9.525 mm, R_y = 9.525 mm, η_0 = 0.06493 Pa·s, α = 14 GPa^{-1}, s_0 = 1.01, ρ_0 = 1037.7 kg/m^3, T_0 = 60 °C. Figure 4 shows the comparisons of the calculated central film thickness (h_{cen}) with the experimental results of Ref. [47] under various entrainment velocities at pure rolling condition. Figure 4 shows that the central film thickness obtained from the mixed TEHL model corresponds closely to measurements at different entrainment speeds. At high speed, the central

Table 1 Contacting bodies and lubricant properties parameter for the validation case

Parameter	Value
Elastic modulus of ball	206 GPa
Elastic modulus of disc	75 GPa
Poisson's ratio of ball	0.3
Poisson's ratio of disc	0.22
Specific heat of ball	470 J/(kg·K)
Specific heat of disc	840 J/(kg·K)
Specific heat of lubricant	2000 J/(kg·K)
Density of ball	7850 kg/m^3
Density of disc	2500 kg/m^3
Density of lubricant	876 kg/m^3
Thermal conductivity of ball	46 W/(m·K)
Thermal conductivity of disc	0.78 W/(m·K)
Thermal conductivity of lubricant	0.14 W/(m·K)
Ambient viscosity of lubricant	1.315 Pa·s
Viscosity–pressure coefficient	24 GPa^{-1}
Ambient temperature	20 °C

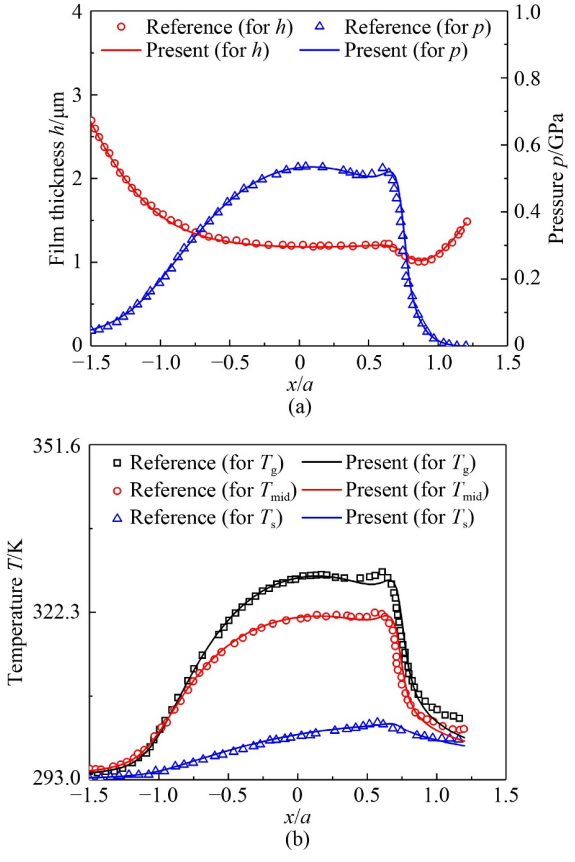

Fig. 3 Present simulations compared with the numerical results from Ref. [46]: (a) centerline pressure and film thickness distributions, (b) centerline temperature distributions.

film thickness of the mixed isothermal EHL model greatly deviates from the measured data because the apparent thermal effect occurs at a high speed, resulting in the decrease of film thickness.

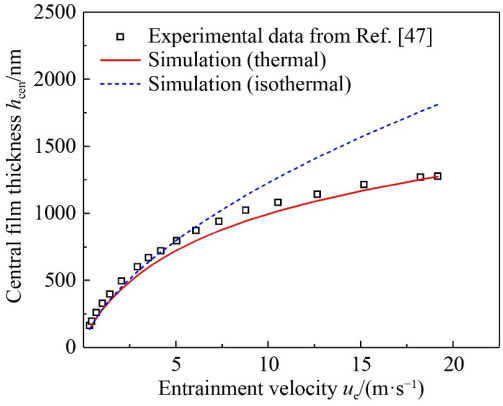

Fig. 4 Comparison of central film thickness between simulations and experimental data in Ref. [47] at different entrainment velocities.

4 Results and discussion

4.1 TEHL with smooth surface

In this section, the effect of *SRR* on TEHL performance is investigated under different applied loads without considering surface roughness. Entrainment velocity is fixed at 20 m/s. Hertzian contact ellipticity of $k = 2$ is selected with the equivalent radii of $R_x = 12.70$ mm and $R_y = 36.13$ mm.

The applied load changes from 170 to 4600 N, and the corresponding maximum Hertzian pressure (p_h) and Hertzian contact radius are shown in Table 2. The properties of the solids and lubricant used for the simulation are given in Table 3, in which the boundary friction coefficient is assumed to be a constant 0.115 based on the friction test data from Ref. [48]. In mixed lubrication analysis, the boundary friction coefficient is commonly set to be a constant, and this value can be determined experimentally, typically between 0.07 and 0.15 for lubricated steel–steel interfaces in engineering practice [48]. The calculation domain is taken as $x_{in} = -3a$, $x_{out} = 1.5a$, $y_{in} = -3a$, $y_{out} = -3a$, and $d = 2a$. A uniform grid of 256 × 256 is adopted in the x and y directions. The computation grid in the z direction consists of 30 uniform grids in oil film and 60 uniform grids in each solid. The dimensionless time step length is taken as $\Delta t = 0.5\Delta X$, where ΔX is the dimensionless mesh size in the x direction.

Figure 5 presents the variations of film thickness with the change in *SRR* under different applied loads. The central film thickness of the thermal model increases first and then decreases with continuously increasing *SRR* due to the thermal expansion of lubricant at low *SRR* (less than about 0.3) [38]. This phenomenon appears more

evident under heavy-load conditions. When *SRR* is high, the thermal thinning of the lubricant becomes dominant, leading to a reduction in central film thickness. Unlike the central film thickness, the minimum film thickness generally keeps decreasing with the increase of *SRR*, except that a slight increase may be seen at low *SRR* if the load is high. As for the change in the pressure, *SRR* appears to have a limited effect on the maximum pressure, but a high *SRR* can cause an increase in secondary pressure peak.

Figure 6 presents the influence of *SRR* on temperature under the load of 2 GPa. With an increased *SRR*, the temperatures in the central film substantially increase, especially in the center of contact area, and the high-temperature zone moves from inlet to contact center. When *SRR* increases from 0 to 1, the film temperature in the center of contact area increases by about 406% because the large lubricant shear heat takes place in the center of contact area with the increase of *SRR*. For the temperature distributions, the temperature drops sharply when the lubricant approaches the outlet region due to the decompression cooling effect, and eventually, the film temperature increases slightly again due to the action of weak shear heat and the disappearance of decompression work [49]. In addition, as shown in Fig. 6, the slower moving surface results in a higher temperature than the faster moving surface because the heat is removed more effectively by the faster surface, and this tendency becomes more apparent as *SRR* increases.

Figure 7 further presents the influence of applied load on temperature under *SRR* of 0.02. The maximum temperatures in the central film and contact surfaces gradually increase linearly when the load increases. For the central film temperature distributions, with the increasing value of the load, the temperatures in the inlet and outlet increase slightly, and the increase in the temperature of the contact center is more apparent. When the applied load increases from 1 to 3 GPa, the film temperature in the center of contact area increases by about 67% because the increasing load clearly increases the shear heat in the center of contact zone, whereas the increase of shear heat in the inlet and outlet is slight. Figure 7(b) shows that although the change in maximum temperature of the slower surface and faster surface increases with the increase of applied load, the difference between the maximum temperature of the two surfaces is not evident under these loading cases.

Table 2 Parameters of Hertzian contact at different applied loads

Applied load, w/N	Maximum Hertzian pressure, p_h/GPa	Hertzian contact radius, a/mm
170	1.0	0.201
580	1.5	0.302
1360	2.0	0.402
2650	2.5	0.502
4600	3.0	0.603

Table 3 Properties of contacting bodies and lubricant

Parameter	Value
Elastic modulus of solids	206 GPa
Poisson's ratio of solids	0.3
Density of solids	7850 kg/m^3
Density of lubricant	971.2 kg/m^3
Specific heat of solids	470 J/(kg·K)
Specific heat of lubricant	1910 J/(kg·K)
Ambient viscosity of lubricant	0.0246 Pa·s
Viscosity–pressure coefficient	18.458 GPa^{-1}
Viscosity–temperature coefficient	0.032 K^{-1}
Thermal conductivity of solids	46 W/(m·K)
Thermal conductivity of lubricant	0.152 W/(m·K)
Thermal expansion coefficient of lubricant	0.000788 K^{-1}
Boundary lubrication friction coefficient	0.115
Ambient temperature	40 °C

4.2 TEHL with surface roughness

In reality, the contact surfaces of mechanical components are not ideally smooth, and their surface failures are correlated closely with the roughness. The roughness effect needs to be considered in TEHL analysis. In this

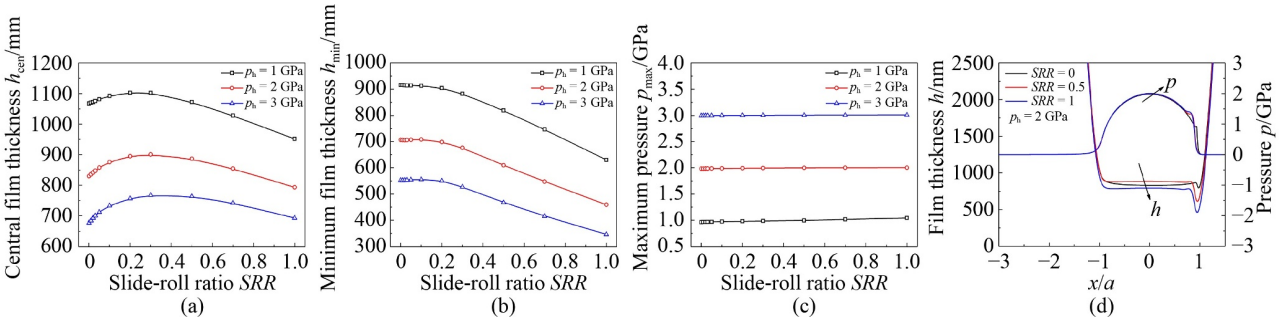

Fig. 5 Effect of *SRR* on film thickness and pressure under different load levels when u_e = 20 m/s: (a) central film thickness, (b) minimum film thickness, (c) maximum pressure, and (d) centerline film thickness and pressure distributions for p_h = 2 GPa.

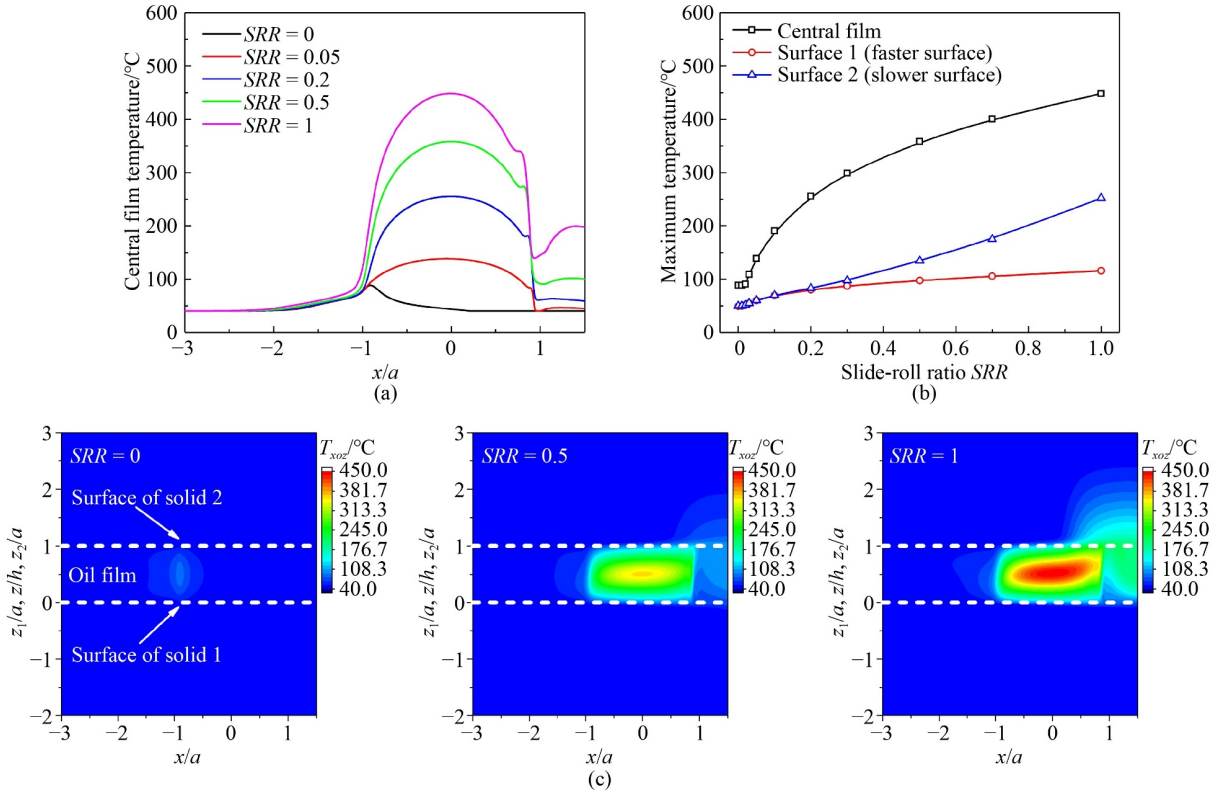

Fig. 6 Effect of *SRR* on temperature when u_e = 20 m/s and p_h = 2 GPa: (a) central film temperature distributions in the rolling direction at y = 0, (b) maximum temperature, and (c) temperature distributions in the x-o-z cross section at y = 0.

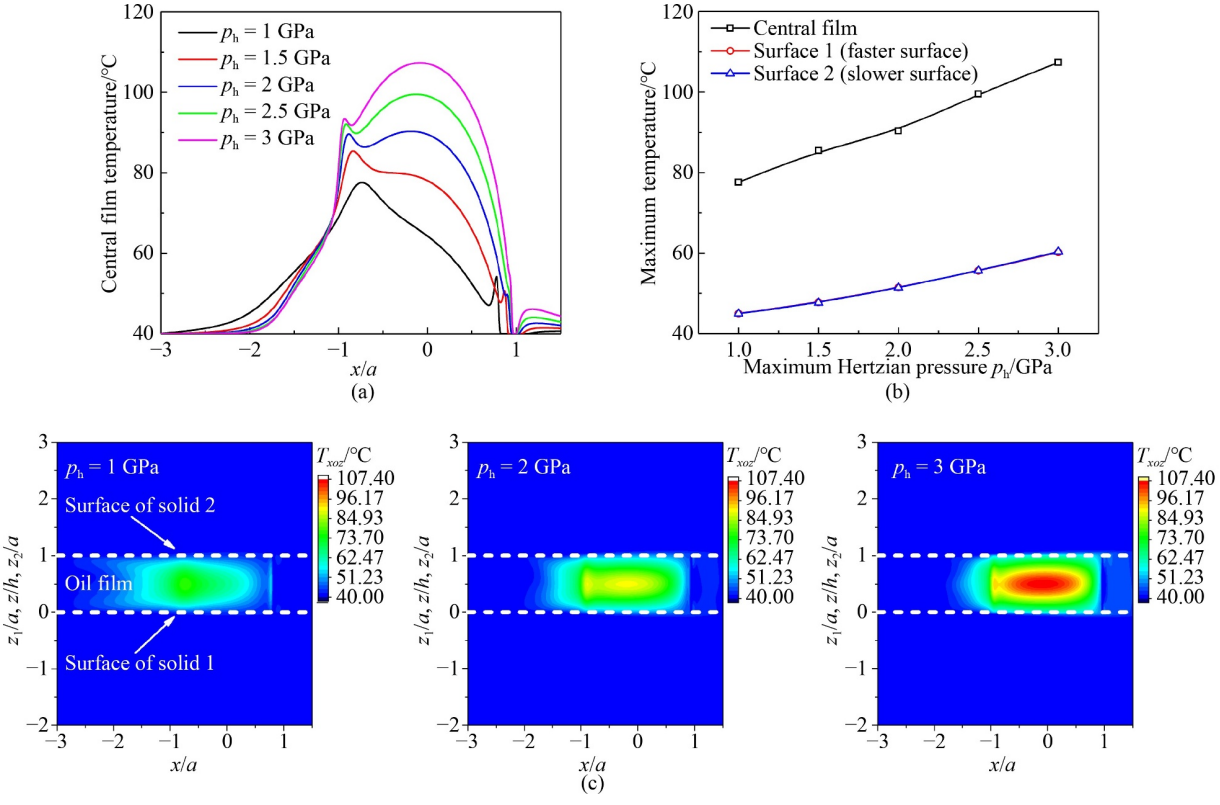

Fig. 7 Effect of load on temperature when u_e = 20 m/s and *SRR* = 0.02: (a) central film temperature distributions in the rolling direction at y = 0, (b) maximum temperature, and (c) temperature distributions in the x-o-z cross section at y = 0.

section, two transversely grinding surfaces with 3D roughness topography are adopted to investigate the roughness effect on the TEHL behaviors, as illustrated in Fig. 8. The root–mean–square roughness value of each surface is set as 0.2 μm. Both rough surfaces have a dimension of 2.6 mm in the x direction and 1.9 mm in the y direction with 2937 × 1881 grid nodes, which are introduced to the computation domain in the form of discretized roughness height data matrix. If the size of rough surfaces is smaller than the Reynolds equation solving domain, the rough surfaces expand by copying themselves in the x and y directions. Figure 8(c) shows a sketch for the mesh discretization in the numerical model. Three computational meshes are employed to improve numerical accuracy when discretizing the rough surfaces, in which the meshes of the moving rough surfaces are denser than those of the stationary solution domain of the Reynolds equation. The roughness heights on the solution domain can be obtained by interpolating among the three meshes, and these height values are renewed as the surfaces move at each time step. Details for handling the rough surfaces can be found in Ref. [50].

Figure 9 shows the comparison of the centerline pressure, film thickness, and central film temperature distributions between rough TEHL and smooth TEHL at different *SRR*s when u_e = 20 m/s and p_h = 2 GPa. Other input parameters are the same as those mentioned in Section 4.1. When the surface is rough, these distributions show large differences compared with those from smooth solutions. Owing to the roughness, considerable variations in film thickness, pressure, and temperature can be seen. At high *SRR*, the maximum pressure is substantially higher than that under pure rolling condition due to the sliding motion of asperities, which is quite different from smooth solutions. With an increased *SRR*, the fluctuations of pressure and temperature caused by the rough surfaces become more remarkable, and the number of peaks of pressure and temperature increase. The contact interface experiences more pressure and temperature peaks during one contact

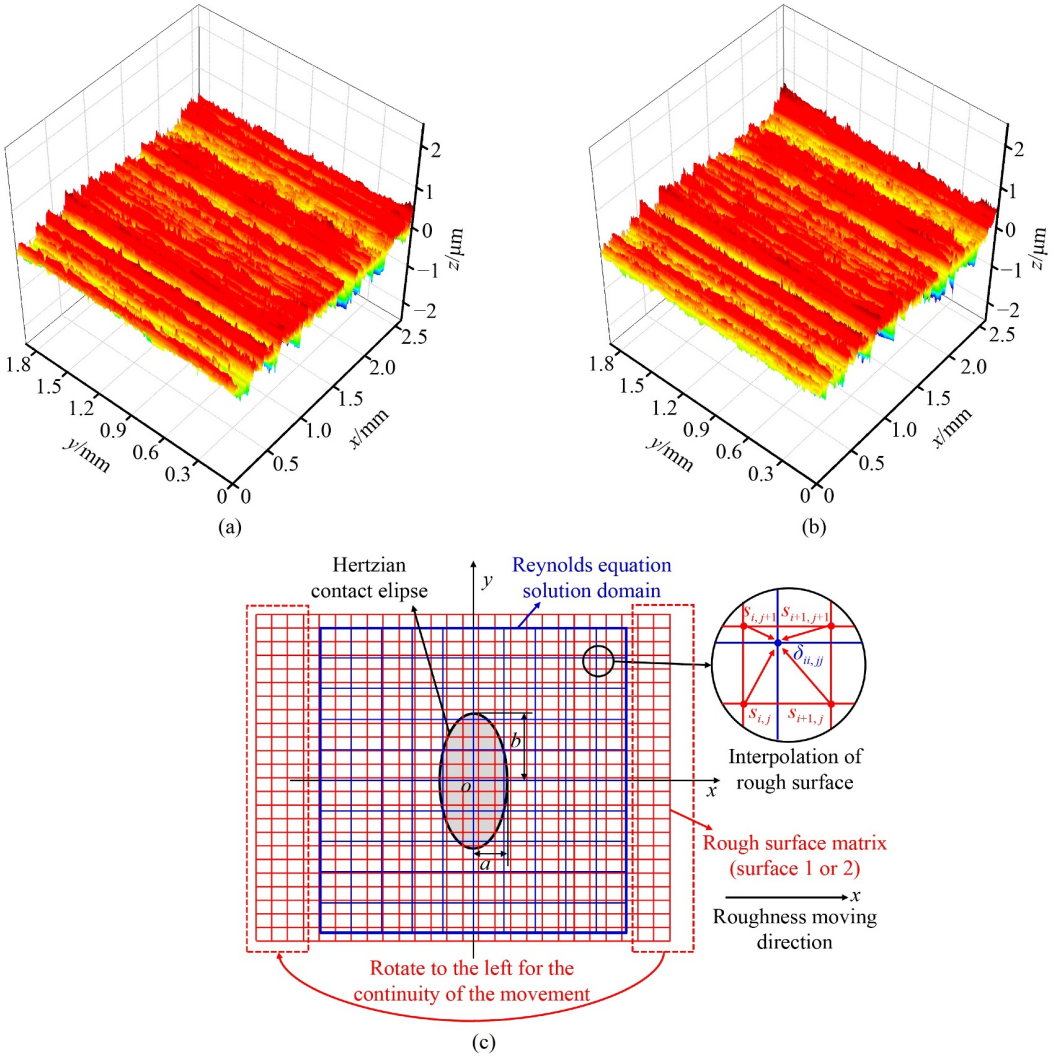

Fig. 8 3D roughness profiles of (a) surface 1 and (b) surface 2. (c) Sketch of mesh discretization in the model.

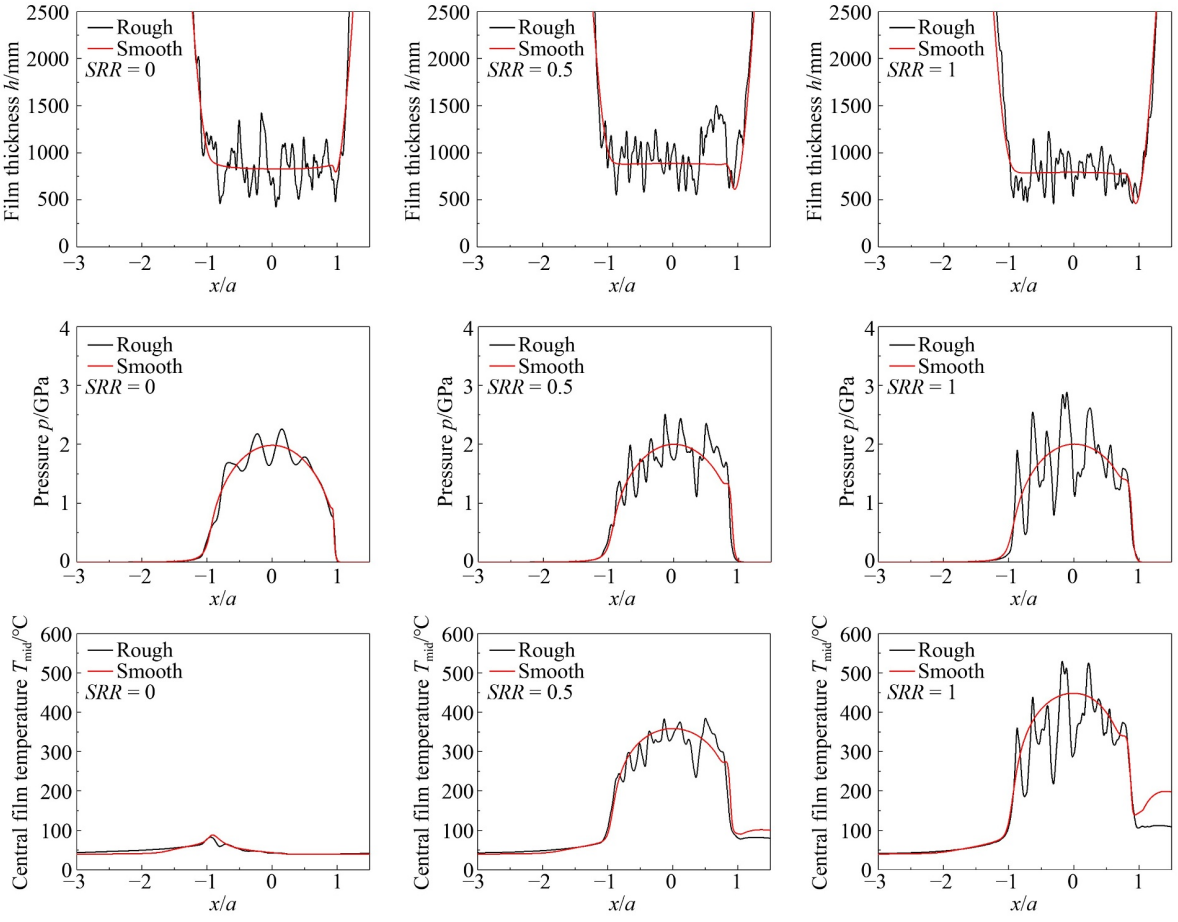

Fig. 9 Comparison of centerline pressure, film thickness, and central film temperature distribution between rough TEHL and smooth TEHL at different *SRR*s when u_e = 20 m/s and p_h = 2 GPa.

cycle, which may accelerate surface failures and shorten contact fatigue life.

Figure 10 shows the comparison of the maximum pressure and minimum film thickness of rough TEHL and smooth TEHL at different loads when u_e = 20 m/s and *SRR* = 0.02. Rough TEHL results in a higher maximum pressure and a smaller minimum film thickness than that of smooth TEHL due to the effect of the surface roughness. Compared with the results of smooth surface, the minimum film thickness with roughness appears to be more sensitive to the change of applied load. Increasing applied load can bring out an evident decrease in minimum film thickness. When load increases to 3 GPa, asperity contacts exist, and the contact interface begins to run in an unsafe mixed lubrication state. Hence, lubrication performance becomes poor, and scuffing failure may occur.

4.3 Effect of speed on TEHL considering surface roughness

High speed may often cause remarkable lubricant shear heat, and this may greatly affect the lubrication behaviors. In this part, a wide range of speed is considered to study its influence on TEHL performance. The entrainment velocity changes from 0.00001 to 100 m/s, covering seven orders of magnitude. The rough surface used is shown in Fig. 8. Other input parameters are the same as those mentioned in Section 4.1.

Figures 11 and 12 show the changes in the mixed TEHL performance at different entrainment velocities when *SRR* = 0.02 and p_h = 2 GPa, which cover the entire lubrication states from boundary and mixed lubrication to full film TEHL. The white areas in the film thickness distributions denote the roughness contacts. Contact load ratio W_c is the ratio of the asperity contact load to the total load, which is used as the criterion for the lubrication status in mixed lubrication analysis. Figure 11 shows that for speeds lower than 0.001 m/s, the contact load ratio is over 82% with severe asperity contacts and insignificant hydrodynamic action, which can be considered the boundary lubrication. When speed is higher than 5 m/s, contact load ratio is almost zero, showing that mixed lubrication is converted to full film lubrication. Under boundary and mixed lubrication conditions at low speeds, the temperature rise of oil film is almost small, and most of the heat generated by the lubricant is diffused into the contact surfaces through heat conduction. Thus,

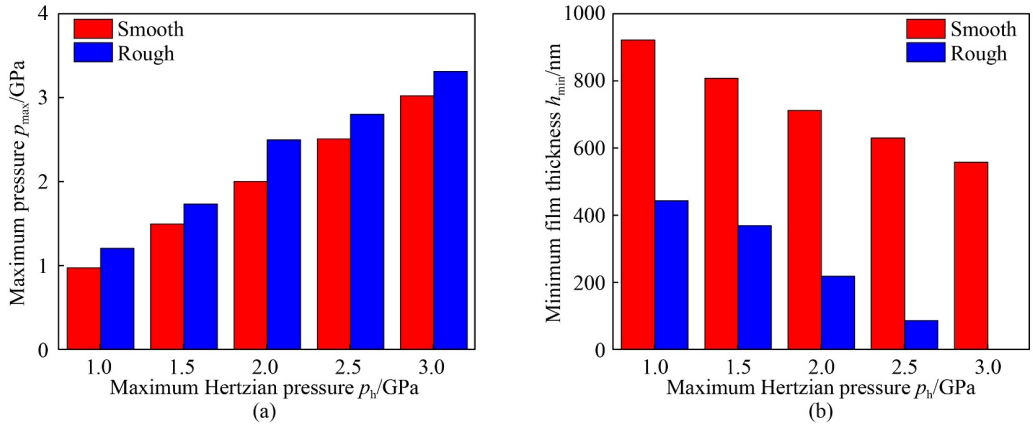

Fig. 10 Comparison of the results between rough TEHL and smooth TEHL at different loads when u_e = 20 m/s and SRR = 0.02: (a) maximum pressure and (b) minimum film thickness.

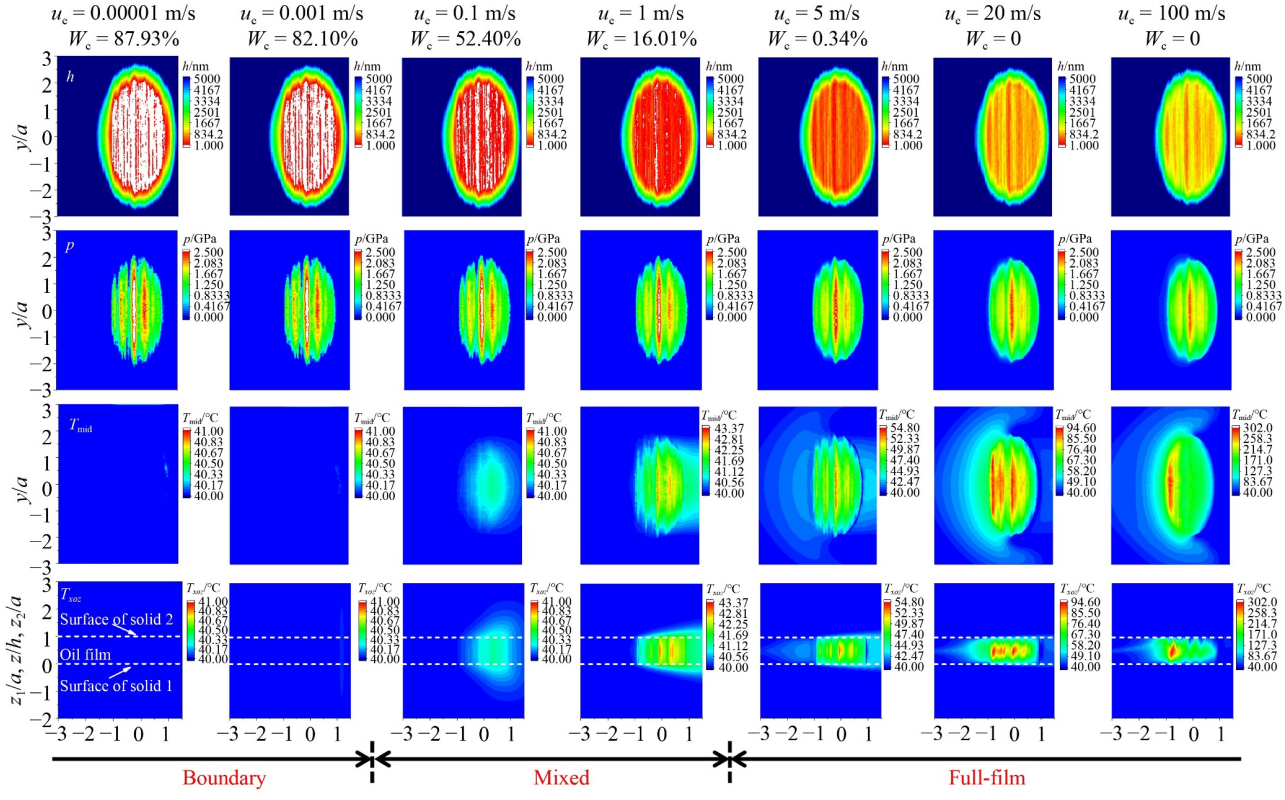

Fig. 11 Variations of film thickness, pressure, and temperature distributions at different entrainment velocities when SRR = 0.02 and p_h = 2 GPa.

the central film temperature approaches the surface temperatures. Under full film lubrication conditions, with the increase of speed, film temperature increases rapidly and becomes much higher than that of contact surfaces. When speed reaches a high level, inlet film temperature changes clearly. Figure 12(a) shows that inlet film temperature appears to be sensitive to the change of speed, showing an evident increase with the increment in speed. This result is due to the reverse flow shear heat. The substantial reverse flow action at high speeds leads to large shear heat generated in the inlet region.

Figures 13 and 14 compare the numerical solutions of mixed TEHL and mixed isothermal EHL at different entrainment velocities. At low speed under the conditions of boundary and mixed lubrication, the results obtained from the isothermal model are close to those from the thermal model as a result of the insignificant thermal effect. With increasing speed under the conditions of full film lubrication, the thermal effect on film thickness and pressure distributions becomes apparent. The film thickness and maximum pressure discrepancy between the two models become increasingly large. When speed

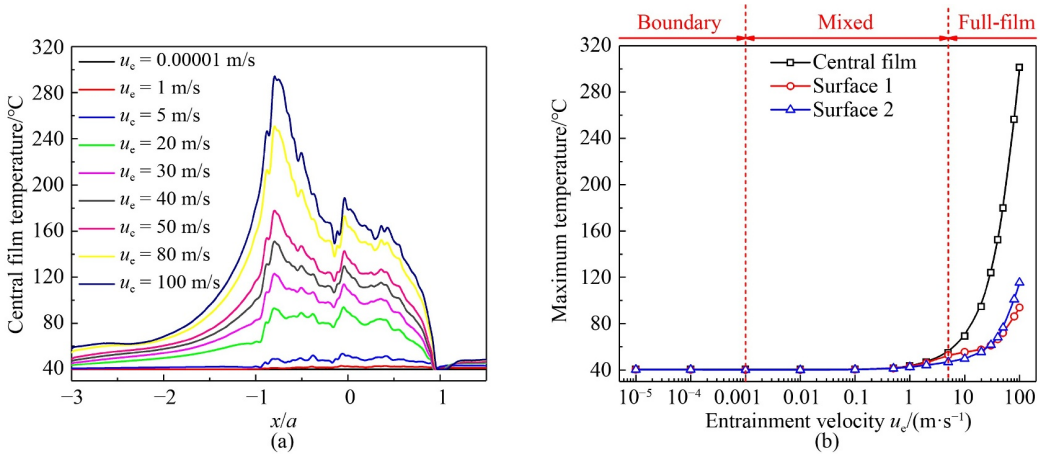

Fig. 12 Effect of entrainment velocity on lubrication performance when SRR = 0.02 and p_h = 2 GPa: (a) central film temperature distributions in the rolling direction at y = 0 and (b) maximum temperature.

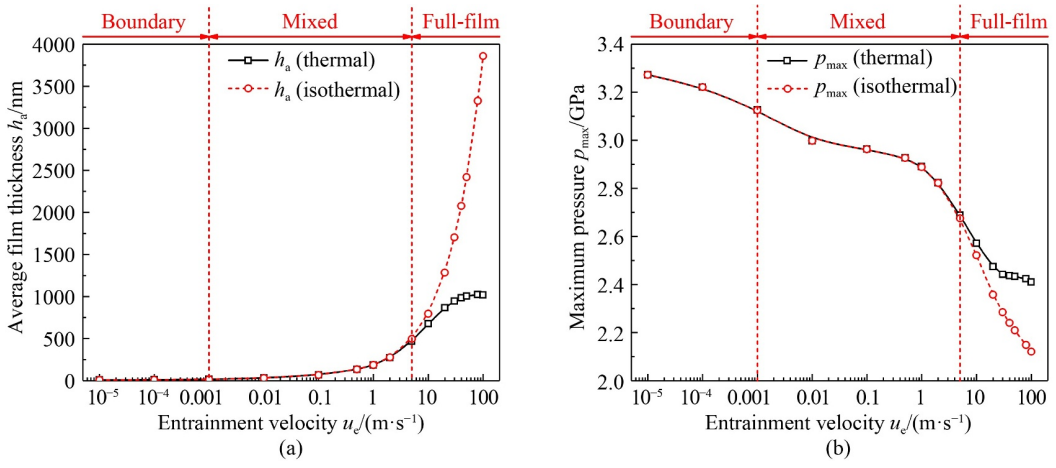

Fig. 13 Comparison of the results between thermal and isothermal models at different entrainment velocities: (a) average film thickness and (b) maximum pressure.

increases to 100 m/s, the deviation of average film thickness and maximum pressure of the two models can reach 279% and 12%, respectively. Figures 13 and 14 show that considerable thermal effect leads to a reduction of lubricant and brings the contacting surfaces closer. Thus, the pressure peaks of the thermal case are higher than those of the isothermal case at some high asperity contact locations. This outcome would result in localized high stresses. Therefore, the isothermal EHL model appears to overestimate the lubrication performance and may not be appropriate in some engineering analyses, such as those rolling bearing and gears serving in high-speed conditions accompanying the substantial thermal effect. Moreover, as speed continuously increases to a high level (higher than 50 m/s or so), the average film thickness obtained from the thermal model does not keep increasing monotonously the same as the isothermal results but remains unchanged because the thermal effect and the entrainment effect have reached a balance. Similar phenomena can be found in the oil film measuring experiments by Zhang et al. [51].

5 Conclusions

A deterministic mixed TEHL model considering real 3D surface roughness and thermal effects is developed. The proposed model is validated with the available data in the literature. The thermal behaviors of 3D rough surface lubricated contacts are investigated over a wide range of running conditions. The associated conclusions are drawn as follows:

(1) With the increment in SRR, the minimum film thickness generally decreases monotonously, whereas the central film thickness first increases and then decreases (SRR > 0.3 or so). Such variation in central film thickness becomes apparent if the load is greater. The increase of SRR and applied load can remarkably increase the film temperature in the center of contact area, and the increase of temperature can reach about 406% and 67% as SRR increases from 0 to 1 and applied load increases from 1 to 3 GPa, respectively. However, the influences of the two

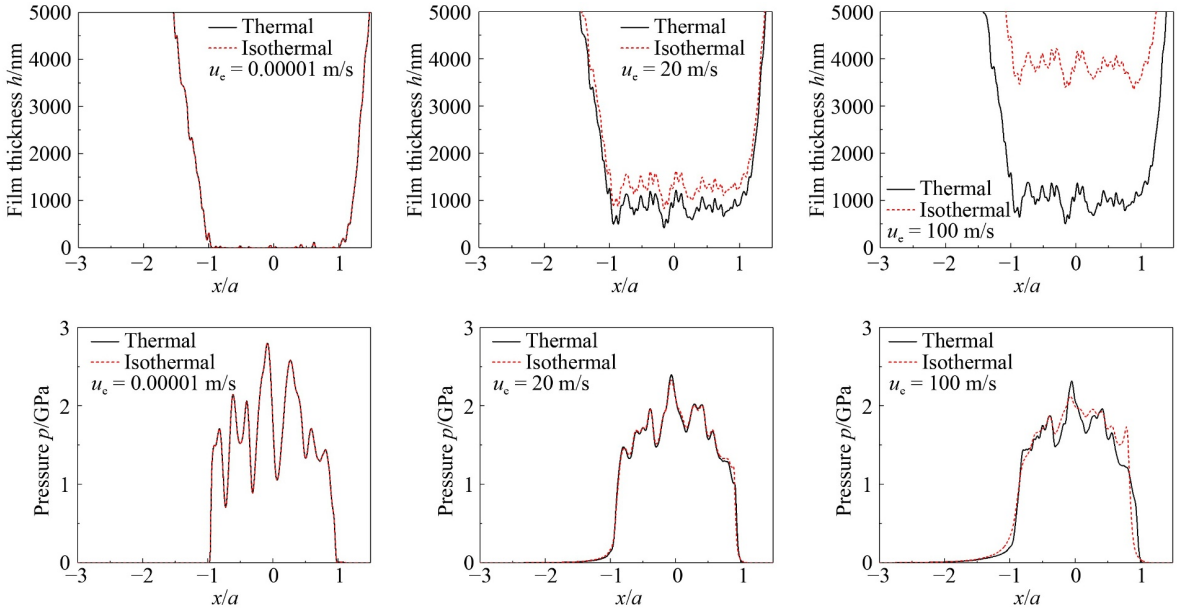

Fig. 14 Comparison of pressure and film thickness profiles at $y = 0$ between thermal and isothermal models with different entrainment velocities when $SRR = 0.02$ and $p_h = 2$ GPa.

parameters on the temperatures in the inlet and outlet are relatively small.

(2) The presence of surface roughness can bring out evident variations in the pressure, film thickness, and temperature distributions. When *SRR* increases, the fluctuations of pressure and temperature become more apparent, and the contact interface experiences more pressure and temperature peaks during one contact cycle.

(3) The rise in inlet temperature is sensitive to the increase of entrainment speed due to the reverse flow shear heat. At a high speed (higher than 5 m/s or so), the average film thickness and maximum pressure of the mixed TEHL model gradually deviates from the results of mixed isothermal EHL model. When speed increases to 100 m/s, the deviation of average film thickness and maximum pressure of the two models can reach 279% and 12%, respectively. Additionally, when speed is higher than a certain value (higher than 50 m/s or so), the thermal film thickness becomes stable due to the balance of thermal effect and entrainment effect.

(4) The proposed mixed TEHL model can simulate the entire transition of interfacial status with real 3D roughness involved, and it can be applied to predict the film thickness, pressure, and temperature of oil film and solids in a wide range of working conditions. However, the mixed TEHL behavior is a complex phenomenon, which is closely related to the material and lubricant properties, working conditions, contact geometry, among other factors. In future work, the effects of starvation and layered materials might be considered in the model to extend the current study.

Acknowledgements This work was supported by the National Key R&D Program of China (Grant No. 2018YFB0703804).

Nomenclature

a, b	Semi axis Hertzian contact ellipse in the x and y directions, respectively
c_1, c_2	Specific heats of solids 1 and 2, respectively
c_f	Specific heat of lubricant
d	Thickness of the temperature calculation domain of solids
E'	Effectively elastic modulus
f_b	Boundary lubrication friction coefficient
h	Film thickness
$h_0(t)$	Rigid body central distance
h_a	Average film thickness
h_b	Boundary film thickness
h_{cen}	Central film thickness
h_{min}	Minimum film thickness
k	Hertzian contact ellipticity
k_1, k_2	Thermal conductivities of solids 1 and 2, respectively
k_f	Thermal conductivity of lubricant
p	Pressure
p_h	Maximum Hertzian pressure
q	Lubricant velocity in the z direction
R_x, R_y	Equivalent radius of contact surfaces in the x and y directions, respectively
s_0	Coefficient for Roelands equation
$s_1(x, y)$, $s_2(x, y)$	Discretized roughness height data matrix of surfaces 1 and 2, respectively
SRR	Slide–roll ratio
t	Time

Δt	Dimensionless time step length
T	Temperature
T_0	Ambient temperature
T_g	Temperature on the surface of glass
T_m	Mean temperature of oil film
T_{mid}	Central film temperature
T_s	Temperature on the surface of steel
T_{xoz}	Temperature in the *x*-*o*-*z* cross section
u	Lubricant velocity in the *x* direction
u_1, u_2	Velocities of surfaces 1 and 2, respectively
u_e	Entrainment velocity
v	Lubricant velocity in the *y* direction
$V_e(x, y, t)$	Elastic deformation
w	Applied load
W_c	Contact load ratio
x	Coordinate in entrainment direction
x_{in}, x_{out}	Inlet and outlet edges in the *x* direction, respectively
ΔX	Dimensionless mesh size in the *x* direction
y	Coordinate perpendicular to entrainment direction
y_{in}, y_{out}	Inlet and outlet edges in the *y* direction, respectively
z	Vertical coordinate across oil film
z_0	Coefficient for Roelands equation
z_1, z_2	Vertical coordinates for solids 1 and 2, respectively
α	Viscosity–pressure coefficient
β	Thermal expansion coefficient of lubricant
γ	Viscosity–temperature coefficient
$\delta_1(x, y, t)$, $\delta_2(x, y, t)$	Roughness heights of surfaces 1 and 2, respectively
ε_p, ε_w, ε_T	Convergence factors of pressure, load, and temperature, respectively
η	Lubricant viscosity
η_0	Ambient viscosity of lubricant
η^*	Lubricant effective viscosity
ξ	*x* coordinate of pressure when calculating deformation
ρ	Lubricant density
ρ_0	Ambient density of lubricant
ρ_1, ρ_2	Densities of solids 1 and 2, respectively
ς	*y* coordinate of pressure when calculating deformation
τ	Shear stress
τ_0	Characteristic shear stress

References

1. Cheng H S, Sternlicht B. A numerical solution for the pressure, temperature, and film thickness between two infinitely long, lubricated rolling and sliding cylinders, under heavy loads. Journal of Basic Engineering, 1965, 87(3): 695–704
2. Zhu D, Wen S Z. A full numerical solution for the thermoelastohydrodynamic problem in elliptical contacts. Journal of Tribology, 1984, 106(2): 246–254
3. Kim K H, Sadeghi F. Three-dimensional temperature distribution in EHD lubrication: part I-circular contact. Journal of Tribology, 1992, 114(1): 32–41
4. Yang P, Qu S, Kaneta M, Nishikawa H. Formation of steady dimples in point TEHL contacts. Journal of Tribology, 2001, 123(1): 42–49
5. Guo F, Yang P R, Qu S Y. On the theory of thermal elastohydrodynamic lubrication at high slide-roll ratios-circular glass-steel contact solution at opposite sliding. Journal of Tribology, 2001, 123(4): 816–821
6. Kaneta M, Yang P. Formation mechanism of steady multi-dimples in thermal EHL point contacts. Journal of Tribology, 2003, 125(2): 241–251
7. Kim H J, Ehret P, Dowson D, Taylor C M. Thermal elastohydrodynamic analysis of circular contacts part 2: non-Newtonian model. Proceedings of the Institution of Mechanical Engineers, Part J: Journal of Engineering Tribology, 2001, 215(4): 353–362
8. Liu X L, Jiang M, Yang P R, Kaneta M. Non-Newtonian thermal analyses of point EHL contacts using the Eyring model. Journal of Tribology, 2005, 127(1): 70–81
9. Cui J, Yang P, Jin Z M, Dowson D. Transient elastohydrodynamic analysis of elliptical contacts. Part 3: non-Newtonian lubricant solution under isothermal and thermal conditions. Proceedings of the Institution of Mechanical Engineers, Part J: Journal of Engineering Tribology, 2007, 221(1): 63–73
10. Liu H J, Zhu C C, Gu Z L, Wang Z J, Tang J Y. Effect of thermal properties of a coated elastohydrodynamic lubrication line contact under various slide-to-roll ratios. Journal of Heat Transfer, 2017, 139(7): 074505
11. Habchi W. On the negative influence of roller-end axial profiling on friction in thermal elastohydrodynamic lubricated finite line contacts. Journal of Tribology, 2020, 142(11): 111601
12. He T, Wang Q J, Zhang X, Liu Y C, Li Z, Kim H J, Pack S. Modeling thermal-visco-elastohydrodynamic lubrication (TVEHL) interfaces of polymer-based materials. Tribology International, 2021, 154: 106691
13. Zhao J X, Sadeghi F, Hoeprich M H. Analysis of EHL circular contact start up: part II—surface temperature rise model and results. Journal of Tribology, 2001, 123(1): 75–82
14. Zhang H B, Wang W Z, Zhang S G, Zhao Z Q. Semi-analytical solution of three-dimensional steady state thermoelastic contact problem of multilayered material under friction heating. International Journal of Thermal Sciences, 2018, 127: 384–399
15. Yang W Y, Zhou Q H, Huang Y Y, Wang J X, Jin X Q, Keer L M. A thermoelastic contact model between a sliding ball and a stationary half space distributed with spherical inhomogeneities. Tribology International, 2019, 131: 33–44
16. Zhang Y G, Wang W Z, Liang H, Zhao Z Q. Layered oil slip model for investigation of film thickness behaviours at high speed conditions. Tribology International, 2019, 131: 137–147
17. Johnson K L, Greenwood J A, Poon S Y. A simple theory of asperity contact in elastohydro-dynamic lubrication. Wear, 1972, 19(1): 91–108

18. Patir N, Cheng H S. An average flow model for determining effects of three-dimensional roughness on partial hydrodynamic lubrication. Journal of Lubrication Technology, 1978, 100(1): 12–17
19. Zhu D, Cheng H S. Effect of surface roughness on the point contact EHL. Journal of Tribology, 1988, 110(1): 32–37
20. Venner C H, ten Napel W E. Surface roughness effects in an EHL line contact. Journal of Tribology, 1992, 114(3): 616–622
21. Chang L, Cusano C, Conry T F. Effects of lubricant rheology and kinematic conditions on micro-elastohydrodynamic lubrication. Journal of Tribology, 1989, 111(2): 344–351
22. Kweh C C, Patching M J, Evans H P, Snidle R W. Simulation of elastohydrodynamic contacts between rough surfaces. Journal of Tribology, 1992, 114(3): 412–419
23. Ai X. Numerical analyses of elastohydrodynamically lubricated line and point contacts with rough surfaces by using semi-system and multigrid methods. Dissertation for the Doctoral Degree. Evanston: Northwestern University, 1993, 56–82
24. Hu Y Z, Zhu D. A full numerical solution to the mixed lubrication in point contacts. Journal of Tribology, 2000, 122(1): 1–9
25. He T, Ren N, Zhu D, Wang J X. Plasto-elastohydrodynamic lubrication in point contacts for surfaces with three-dimensional sinusoidal waviness and real machined roughness. Journal of Tribology, 2014, 136(3): 031504
26. He T, Zhu D, Yu C J, Wang Q J. Mixed elastohydrodynamic lubrication model for finite roller-coated half space interfaces. Tribology International, 2019, 134: 178–189
27. He T, Wang Z J, Wu J Q. Effect of imperfect coating on the elastohydrodynamic lubrication: dislocation-like and force-like coating-substrate interfaces. Tribology International, 2020, 143: 106098
28. He T, Wang Q J, Zhang X, Liu Y C, Li Z, Kim H J, Pack S. Visco-elastohydrodynamic lubrication of layered materials with imperfect layer-substrate interfaces. International Journal of Mechanical Sciences, 2021, 189: 105993
29. Pu W, Wang J X, Yang R S, Zhu D. Mixed elastohydrodynamic lubrication with three-dimensional machined roughness in spiral bevel and hypoid gears. Journal of Tribology, 2015, 137(4): 041503
30. Wang Z Z, Pu W, Zhang Y, Cao W. Transient behaviors of friction, temperature and fatigue in different contact trajectories for spiral bevel gears. Tribology International, 2020, 141: 105965
31. Gan L, Xiao K, Wang J X, Pu W, Cao W. A numerical method to investigate the temperature behavior of spiral bevel gears under mixed lubrication condition. Applied Thermal Engineering, 2019, 147: 866–875
32. Chen S, Yin N, Cai X J, Zhang Z N. Iteration framework for solving mixed lubrication computation problems. Frontiers of Mechanical Engineering, 2021, 16(3): 635–648
33. Wang W Z, Liu Y C, Wang H, Hu Y Z. A computer thermal model of mixed lubrication in point contacts. Journal of Tribology, 2004, 126(1): 162–170
34. Wang W Z, Hu Y Z, Liu Y C, Wang H. Deterministic solutions and thermal analysis for mixed lubrication in point contacts. Tribology International, 2007, 40(4): 687–693
35. Yan X L, Zhang Y Y, Xie G X, Qin F, Zhang X W. Effects of spinning on the mixed thermal elastohydrodynamic lubrication and fatigue life in point contacts. Proceedings of the Institution of Mechanical Engineers, Part J: Journal of Engineering Tribology, 2019, 233(12): 1820–1832
36. Wang X P, Liu Y C, Zhu D. Numerical solution of mixed thermal elastohydrodynamic lubrication in point contacts with three-dimensional surface roughness. Journal of Tribology, 2017, 139(1): 011501
37. Zhu D. On some aspects of numerical solutions of thin-film and mixed elastohydrodynamic lubrication. Proceedings of the Institution of Mechanical Engineers, Part J: Journal of Engineering Tribology, 2007, 221(5): 561–579
38. Kim H J, Ehret P, Dowson D, Taylor C M. Thermal elastohydrodynamic analysis of circular contacts part 1: Newtonian model. Proceedings of the Institution of Mechanical Engineers, Part J: Journal of Engineering Tribology, 2001, 215(4): 339–352
39. Roelands C J A, Vlugter J C, Waterman H I. The viscosity-temperature-pressure relationship of lubricating oils and its correlation with chemical constitution. Journal of Basic Engineering, 1963, 85(4): 601–607
40. Dowson D, Higginson G R. Elasto-hydrodynamic lubrication: the fundamentals of roller and gear lubrication. Oxford: Pergamon Press, 1966
41. Cui J L, Yang P R. Transient thermo-EHL theory of point contact—the process of a bump on the fast surface passing a bump on the slower surface. Tribology Series, 2003, 43: 253–261
42. Shi X J, Wu J Q, Zhao B, Ma X, Lu X Q. Mixed thermal elastohydrodynamic lubrication analysis with dynamic performance of aero ball bearing during start-up and shut-down. Proceedings of the Institution of Mechanical Engineers, Part J: Journal of Engineering Tribology, 2020, 234(6): 873–886
43. Liu S B, Wang Q. Studying contact stress fields caused by surface tractions with a discrete convolution and fast Fourier transform algorithm. Journal of Tribology, 2002, 124(1): 36–45
44. Liu S B, Wang Q, Liu G. A versatile method of discrete convolution and FFT (DC-FFT) for contact analyses. Wear, 2000, 243(1−2): 101–111
45. Guo F, Yang P, Wong P L. On the thermal elastohydrodynamic lubrication in opposite sliding circular contacts. Tribology International, 2001, 34(7): 443–452
46. Kaneta M, Yang P, Hooke C J. Effects of the thermal conductivity of contact materials on elastohydrodynamic lubrication characteristics. Proceedings of the Institution of Mechanical Engineers, Part C: Journal of Mechanical Engineering Science, 2010, 224(12): 2577–2587
47. Liang H, Guo D, Reddyhoff T, Spikes H, Luo J B. Influence of thermal effects on elastohydrodynamic (EHD) lubrication behavior at high speeds. Science China Technological Sciences, 2015, 58(3): 551–558
48. He T, Zhu D, Wang J X, Wang Q J. Experimental and numerical investigations of the stribeck curves for lubricated counterformal contacts. Journal of Tribology, 2017, 139(2): 021505
49. Sun H Y, Yang P R, Chen X Y. Study on abnormal temperature field of slide/roll contact under elastohydrodynamic lubrication. Tribology, 2004, 24(1): 66−69 (in Chinese)
50. Zhu D, Liu Y C, Wang Q. On the numerical accuracy of rough surface EHL solution. Tribology Transactions, 2014, 57(4): 570–580
51. Zhang Y G, Wang W Z, Zhang S G, Zhao Z Q. Experimental study of EHL film thickness behaviour at high speed in ball-on-ring contacts. Tribology International, 2017, 113: 216–223